Available online at www.sciencedirect.com

SciVerse ScienceDirect

Ceramics International 38 (2012) 1627–1633

CERAMICS INTERNATIONAL

www.elsevier.com/locate/ceramint

Mechanical properties at nanometric scale of alumina layers formed in sulphuric acid anodizing under burning conditions

J.J. Roa [a,*], B. Gastón-García [b], E. García-Lecina [b], C. Müller [c]

[a] *Institut P' (UPR 3346), Département de Physique et Mécanique des Matériaux, CNRS – Université de Poitiers – ENSMA, Boulevard Marie et Pierre Curie, SP2MI – Téléport 2 – BP 30179, F-86962 Futuroscope Chasseneuil Cedex, France*

[b] *Surface Finishing Department, CIDETEC-IK4, P° Miramón 196, E-20009 San Sebastián, Spain*

[c] *ELECTRODEP, Departament de Química Física, Facultat de Química, Universitat de Barcelona, C/Martí i Franquès 1, E-08028 Barcelona, Spain*

Received 29 August 2011; received in revised form 27 September 2011; accepted 27 September 2011
Available online 5 October 2011

Abstract

A mechanical study (hardness, H and Young's modulus, E) at nanometric scale of the distribution of mechanical properties across the surface of porous anodic alumina (PAA) films formed during aluminium anodizing in sulphuric acid under burning conditions is presented. Statistical methods have been employed to extract the mechanical properties of the protruding oxide structures (POS) observed in the burning areas and the results have been compared with those obtained from the standard PAA (S-PAA) of the non-burning areas. The results indicated that H and E of the POS are 3.8 ± 0.3 and 80 ± 4 GPa, respectively, while those of the S-PAA are 6.8 ± 0.5 and 125 ± 8 GPa. Thus, the hardness and Young's modulus of POS are factors of about 1.6–1.8 times lower than those of S-PAA, indicating that POS have lower mechanical properties associated with their different chemical composition and structure.

Keywords: Hardness; Nanoindentation technique; Statistical method; Anodizing process

1. Introduction

Anodizing process has been widely adopted in industry to improve the properties of aluminium and its alloys, as it allows the growth of an alumina film on the aluminium substrate with excellent corrosion resistance and mechanical characteristics [1].

Porous anodic alumina (PAA) films formed by this technique in acid electrolytes are characterized by very uniform morphology: cylindrical pores perpendicular to the metal surface, arranged in a close-packed hexagonal structure and separated from the substrate by a compact barrier layer. The pore and cell size determine the features of the PAA film and can be modulated by a suitable selection of the aluminium alloy and the control of the anodizing conditions [2]. However, under certain operating conditions, film nonuniformity occurs giving rise to local anodic film thickening in the form of protruding oxide structures (POS). This local phenomenon, commonly known as burning, is easily detectable from the rest of the surface by the observation of randomly distributed spots with a whitish (in the case of sulphuric or phosphoric acid anodizing) or blackish (in the case of organic acid anodizing) colour [3–5]. Up to now, burning phenomenon is not well established but its initiation seems to be associated with the attainment of a certain critical voltage sensitive to the electrolyte nature and the anodizing conditions [6], and the development of very high local anodic current densities which lead to a considerably increase in local temperature [7–11]. As a consequence of chemical and structural differences [12], the mechanical properties of the hillocks may differ from those of the standard PAA (S-PAA). However, the mechanical properties of these structures are unknown due to the difficulty and unaccuracy of mechanical measurements of small volumes by conventional techniques.

In this sense, Instrumented Indentation Technique (IIT), also known as nanoindentation, has recently attracted significant research interest for measuring the mechanical properties of materials at nanometric scale [13,14], because its various advantages such as non-destructive specimen preparation, easy process and high spatial resolution. Like a traditional hardness test, by IIT an indenter with a well-defined geometry is forced

* Corresponding author.
E-mail address: jjrr_cons@hotmail.com (J.J. Roa).

0272-8842/$36.00
doi:10.1016/j.ceramint.2011.09.053

into the surface of a sample using a known force. In contrast to traditional hardness testers, IIT utilized high-resolution instrumentation to continuously monitor and control the displacement of the indenter as it penetrates into and is withdrawn from the sample, allowing a simple estimation of hardness (H) and Young's modulus (E) [15].

Thus, this study presents novel results on the utilization of nanoindentation to investigate the nanomechanical properties of the heterogeneous alumina layers formed during anodizing in sulphuric acid under burning conditions. In particular the study is focused on the nanomechanical differences between the POS and the S-PAA observed in the non-burning areas. Statistical method [16–21] was employed to clarify and isolate the mechanical properties of each phase (S-PAA, POS and S-PAA/$POS_{interface}$) in order to relate them with their composition and structure. The results will contribute to a better understanding of the characteristics of alumina layers formed in anodizing processes under burning conditions.

2. Experimental procedure

2.1. Sample preparation

PAA layers were obtained using as-received commercial sheets of laminated AA1050 aluminium alloy (99.5% Al, with Fe (<0.40%) and Si (<0.25%) as main alloying elements) (14.3 cm^2). Prior to anodizing, aluminium specimens were pretreated following a 5-step procedure [22]: (i) alkaline degreasing in Almeco Clean® (Henkel), (ii) alkaline etching in a $NaOH/NaC_6H_{11}O_7$ solution at 55 °C, (iii) desmutting in HNO_3 30% at room temperature, (iv) galvanostatic electropolishing in H_3PO_4/H_2SO_4 solution at 77.5 °C and (v) acid etching in H_3PO_4/CrO_3 at 55 °C. Samples were thoroughly rinsed in distilled water after each step.

Without delay, a single-step galvanostatic anodizing at 1.5 A dm^{-2} was carried out in a 1.2 M sulphuric acid electrolyte at 10 °C for 40 min. Anodizing was conducted in a thermostatized two-electrode cell (1.5 L) with a cylindrical lead cathode and agitation by air. Temperature of the electrolyte was controlled with a cryostat device (Julabo F12-MC) (±0.02 °C). The current was applied by a direct current power supply (Delta SM300-5) and the evolution of the voltage during anodization was measured and transferred to a computer by a multimeter (Agilent HP34401A). Surface morphology and cross-section structure of the PAA layers were analyzed by scanning electron microscopy (SEM) (Hitachi S-2300) and atomic force microscopy (AFM) (Digital Instruments Multimode) in tapping mode and the images were treated using WSxM software [23]. For the chemical analysis of the anodic films an electron probe microanalyzer (EPMA) (Cameca SX50) was used.

2.2. Mechanical tests

Nanoindentation tests were performed using a NHT apparatus from CSM (Peseux, Switzerland) equipped with a Berkovich tip indenter with a 20 nm of radius. The indenter shape was calibrated by indenting fused silica samples of known Young's modulus value of 72 GPa [13]. In order to isolate the mechanical properties of the POS and the S-PAA, an array of 1024 imprints (32 × 32 with a constant spacing of 4 μm) was performed at 150 nm of penetration depth (h) in the longitudinal direction. The loading/unloading curves (or P–h curve) for each experiment were recorded, and H and E were directly extracted from the linear part of the unloading curve using the Oliver and Pharr method [13,24–26]. Part of the nanoindentation array has been observed using the optical microscope coupled to the nanoindenter.

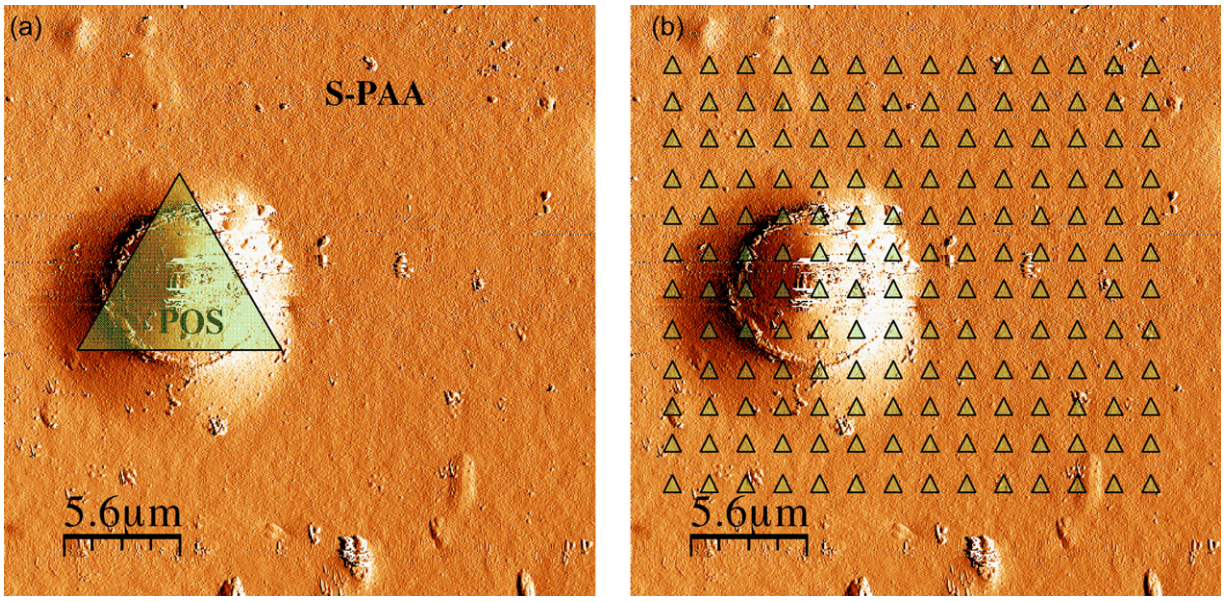

Fig. 1. Statistical method sampling illustration over a POS and S-PAA sample. Adapted from Constantinides et al. [16,18,19].

2.3. Statistical approach

The scheme presented in Fig. 1 helps to better understand the different advantages associated with the statistical method for heterogeneous materials like the material of study. Here the most important parameter to take into account is the indentation depth chosen to perform the different experiments. During the last years, Constantinides and co-workers [16,18,19] have proposed the following classification for heterogeneous materials composed by several phases having each one their own mechanical properties and a characteristic diameter.

(i) *High indentation depths (or high applied loads)*: At high indentation depths or applied loads, the different phases cannot be isolated as the residual imprint is higher than the size of each secondary phase. Thus, the recorded response will correspond to the response of the whole material, neglecting the contribution of each phase, and yielding only one Gaussian distribution peak. This behaviour is represented in Fig. 1a by a big sized triangle over the AFM image.

(ii) *Low indentation depths (or low applied loads)*: When the nanoindentation tests are carried out at small scale, the contribution of each phase present in the sample of study can be isolated as the size of the plastic and elastic field is lower than the size of the phase of study. In this situation, the response of the applied load is represented by three different Gaussian distribution peaks, each one associated to a phase: POS, S-PAA and S-PAA/$POS_{interface}$. This behaviour corresponds to tests performed at small indentation depths, and is represented in Fig. 1b by an array of small triangles over the AFM image.

Finally, it is important to comment that having a large number of indentations will increase the accuracy of the results. In this sense, the different data coming from the nanoindentation tests can be treated and interpreted by means of a statistical approach. Thus, considering a sample composed of different phases (denoted with the letter j) with enough contrast in their mechanical properties (H and E), the distribution of the mechanical properties (p_j) of each phase (x) is assumed to obey a Gaussian distribution [16,18–21,27] denoted with the following equation:

$$p_j = \frac{1}{\sqrt{2\pi\sigma_j^2}} \exp\left[-\frac{(x-\mu_j)^2}{2\sigma_j^2}\right] \quad (1)$$

where σ_j is the standard deviation and μ_j the arithmetic mean for each of the number of indentations (N_j) on the material phases. The cumulative distribution function (CDF) can be calculated using the following equation:

$$\mathrm{CDF} = \sum_j \frac{1}{2} f_j er f\left(\frac{x-x_j}{\sqrt{2}\sigma_j}\right) \quad (2)$$

where f_j is the relative fraction occupied by each phase and defined as:

$$f_j = \frac{N_j}{N} \quad (3)$$

where N is the total amount of indentations. Moreover, this relative fraction must obey to the following equation:

$$\sum_{j=1}^{n} f_j = 1 \quad (4)$$

Once the experimental CDF is obtained, a deconvolution process is applied and the mechanical properties of each phase (POS, S-PAA and POS/S-$PAA_{interface}$) present in the sample of study can be estimated.

3. Results and discussion

3.1. Microstructural and chemical analysis

When considering the topography of the PAA films under burning conditions, an undulating surface with protruding oxide hillocks was observed (Fig. 2). In general, these oxide hillocks present a concentric morphology, with the highest point located in the centre and a decreasing oxide thickness towards the border. The height and diagonal length of one of these oxide hillocks are observed in Fig. 3, measured directly from the line traces of an AFM image along the diagonal section of the hillock (between the arrows a and b). The average height and length of the hillock was 1.75 ± 0.25 and 12 ± 4 μm, respectively.

SEM analysis of the cross section of the PAA film, showed that the structure of these hillocks is formed by two main structures (Fig. 4): a protruding oxide structure (POS) (lentil-shaped) where the hexagonal cells are located perpendicular to the substrate and, because of this, with a certain inclination in relation with the surface of the hillock, and a S-PAA layer under the tubular one, with the same thickness and structure as the S-PAA formed in the non-burning area [7,12].

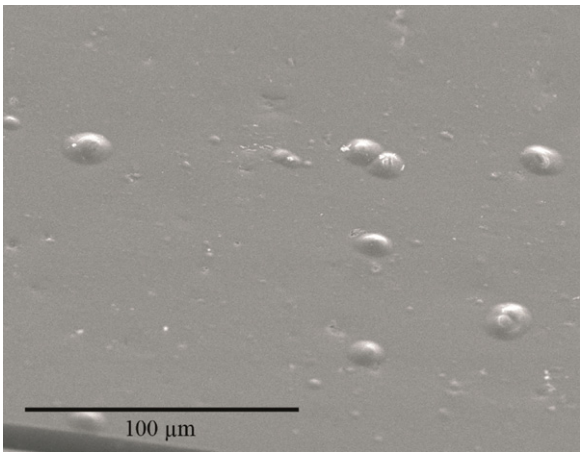

Fig. 2. SEM image of alumina surface with oxide hillocks obtained anodizing under burning conditions.

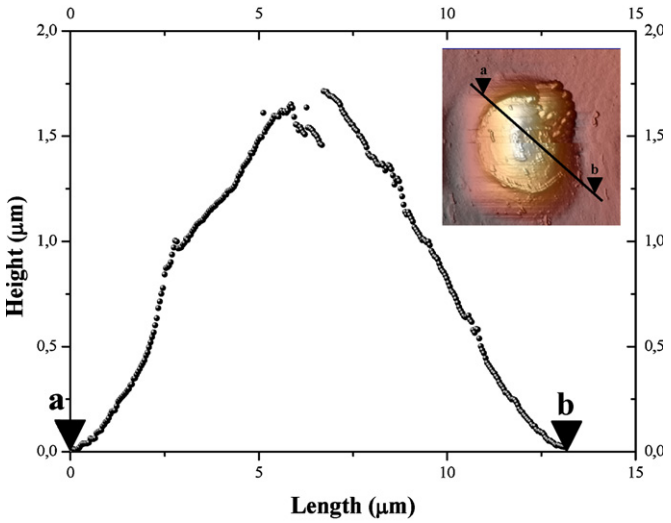

Fig. 3. AFM profile of the oxide hillock shape presented in Fig. 1.

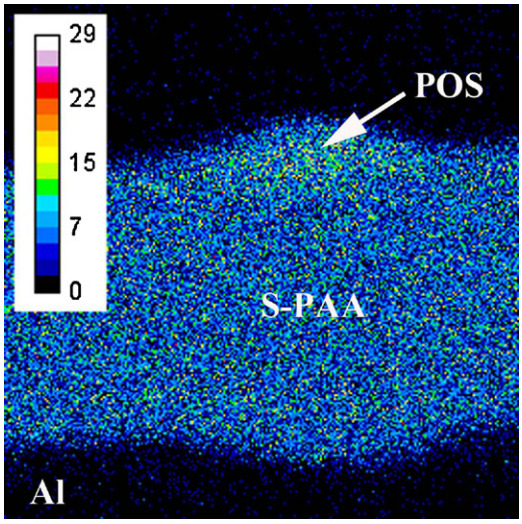

Fig. 5. EPMA maps of sulphur (S) in an oxide hillock obtained after aluminium anodizing under burning conditions.

Besides this, in the case of AA1050 alloy, chemical differences between the different structures of the oxide hillocks have been described [12]. Thus, the POS exhibited lower aluminium and higher sulphur content than the standard PAA layer, as can be seen by electron microprobe analysis (Fig. 5). Moreover, iron and silicon were detected on the top of the hillocks, probably remaining from dissolution of intermetallic particles (Al–Fe–Si or Al–Fe) during substrate pretreatment [12].

3.2. Mechanical properties

3.2.1. Imprints observation

In order to obtain representative distribution of the mechanical properties in the heterogeneous PAA films obtained under burning conditions, a grid of 1024 indentations was performed in the sample of study. Fig. 6 exhibits an optical image (low resolution) of a small part of the indentation array performed by applying 150 nm of indentation depth with a constant distance between each imprint of 4 μm. The different phases of the surface and the different nanoindentation imprints are observed. Thus, POS can be observed randomly distributed in the surface of the sample, so that they can be easily identified and indented separately. It is important to highlight that the size of the POS are higher than the nanoindentation imprints performed at these loads, enabling the separation of each phase, POS and S-PAA. Moreover, the surface of study presents some defects heterogeneously distributed in the surface of study (like porosity, roughness and some secondary phases). All of these defects will be treated as a different phase using the statistical method. This technique allows to extract the mechanical behaviour for each phase without the need of observe with a high resolution each imprint after the indentation process and it yields reduce the time consuming during the treatment data of a high amount of tests.

3.2.2. Statistical method

In order to observe, discuss and obtain the mechanical properties for each phase, we represent the Cumulative Distribution Function (CDF) versus the corresponding mechanical properties, by assuming that the density functions are

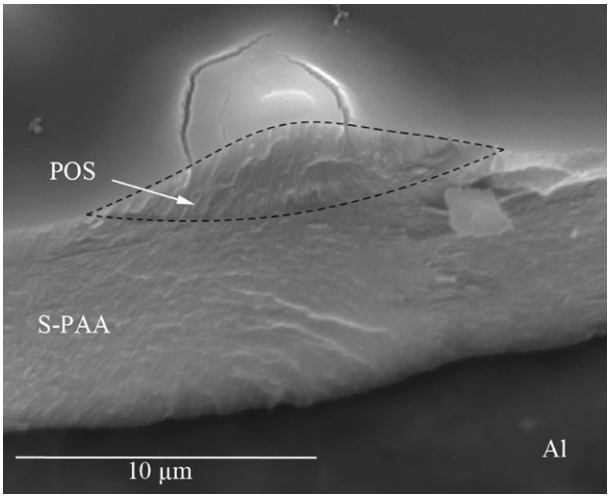

Fig. 4. SEM image of cross-sectioned oxide hillock.

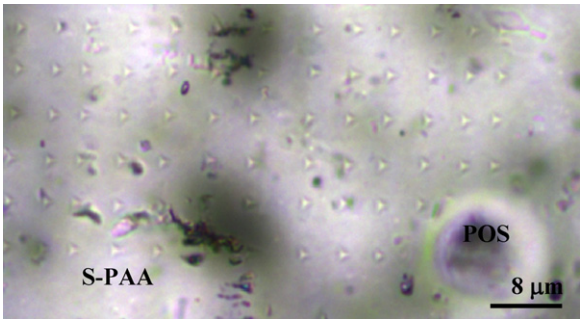

Fig. 6. Optical microscope (OM) micrograph of nanohardness impressions performed at 150 nm of indentation depth.

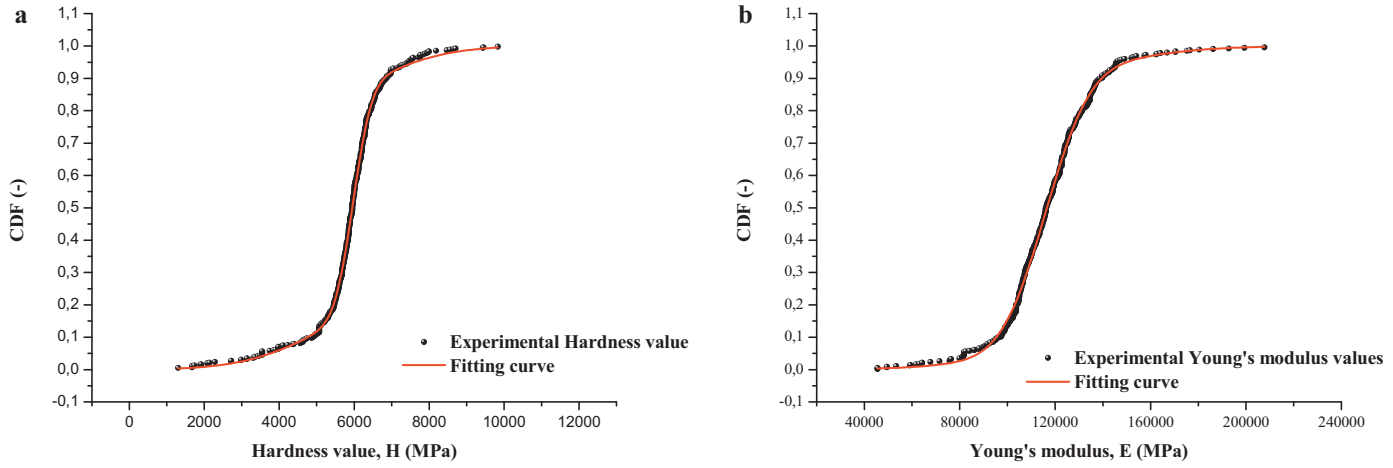

Fig. 7. Statistical analysis: (a) CDF vs. hardness and (b) CDF vs. Young's modulus.

correctly fitted by Gaussian distributions. This approach has also been reported in previous studies performed on heterogeneous materials [16,18–21]. The mean values μ_j^H and μ_j^E, and the standard deviations σ_j^H and σ_j^E, for each mechanical property, H and E distributions, were acquired by fitting the CDF, using a special sigmoid shape error function. For our heterogeneous materials with two different phases (POS and S-PAA) and the interface, the equation 2 can be re-written as:

$$\begin{aligned}\mathrm{CDF} &= \sum_j \frac{1}{2} f_j erf\left(\frac{x - x_j}{\sqrt{2}\sigma_j}\right) \\ &= \frac{1}{2} f_{\mathrm{POS}} erf\left(\frac{x - x_{\mathrm{POS}}}{\sqrt{2}\sigma_{\mathrm{POS}}}\right) + \frac{1}{2} f_{\text{S-PAA}} erf\left(\frac{x - x_{\text{S-PAA}}}{\sqrt{2}\sigma_{\text{S-PAA}}}\right) \\ &\quad + \frac{1}{2} f_{\mathrm{interface}} erf\left(\frac{x - x_{\mathrm{interface}}}{\sqrt{2}\sigma_{\mathrm{interface}}}\right)\end{aligned} \tag{5}$$

During the deconvolution process using Eq. (5) the different mechanical properties for each phase can be obtained. Several restrictions were programmed on the deconvolution: the sum of the total area (f_j) was set 1, and the fitting process was programmed to be completed when the tolerance of the chi-square (χ^2) was less than 1×10^{-15}. Fig. 7 plots the experimental and fitted data for the hardness (Fig. 7a) and Young's modulus (Fig. 7b) CDF curves. One of the most important things using this statistical method is that we can extract the mechanical properties for each phase without the need to observe the different imprints. The results obtained after the deconvolution process are summarized in Table 1.

The histogram of H and E values, measured with the same penetration depth using a constant bin size of 500 MPa, is presented in Fig. 8a and b, respectively. Two main peaks are observed in both distributions. The highest one, centred at 6.8 ± 0.5 GPa for H and 125 ± 8 GPa for E, respectively, was ascribed to the S-PAA structure. The lowest was ascribed to the POS, based on, as we can see in Table 1, the fraction of surface area covered by this phase is lower than that corresponding to S-PAA, leading to H and E values of 3.8 ± 0.3 GPa and 80 ± 4 GPa, respectively. The intermediate value is ascribed to the POS/S-PAA$_{\mathrm{interface}}$, yielding H and E values of 4.2 ± 0.4 GPa and 95 ± 6 GPa, respectively. Thus, the hardness and Young's modulus of POS are factors of about 1.6–1.8 times lower than those of S-PAA, indicating that POS have lower mechanical properties, derived from their different chemical composition and structure. The results would also indicate that porous anodic alumina that surrounds the POS (POS/S-PAA$_{\mathrm{interface}}$) presents a degradation of their mechanical properties, probably due to mechanical stresses arising from the expansionary forces originated by the rapid oxide growth of POS in relation with S-PAA.

The mechanical parameters of S-PAA measured here are close to the results reported for other nanoporous anodic alumina films, which are typically in the range of 4–6 GPa for the hardness and 100–140 GPa for the Young's modulus [28,29] The small differences among the data could be attributed to the different technique employed to extract these parameters

Table 1
Summary of the different results obtained after the CDF fitting for each phase.

Phase	GPa		%	Adj. R^2	χ^2	GPa		%	Adj. R^2	χ^2
	μ^H	σ^H	f_j			μ^E	σ^E	f_j		
POS	3.8	0.3	20.4	0.9973	9.64×10^{-5}	80	4	15.3	0.9981	3.02×10^{-4}
S-PAA	6.8	0.5	65.3			125	8	55.6		
POS/S-PAA$_{\mathrm{interface}}$	4.2	0.4	14.3			95	6	29.1		

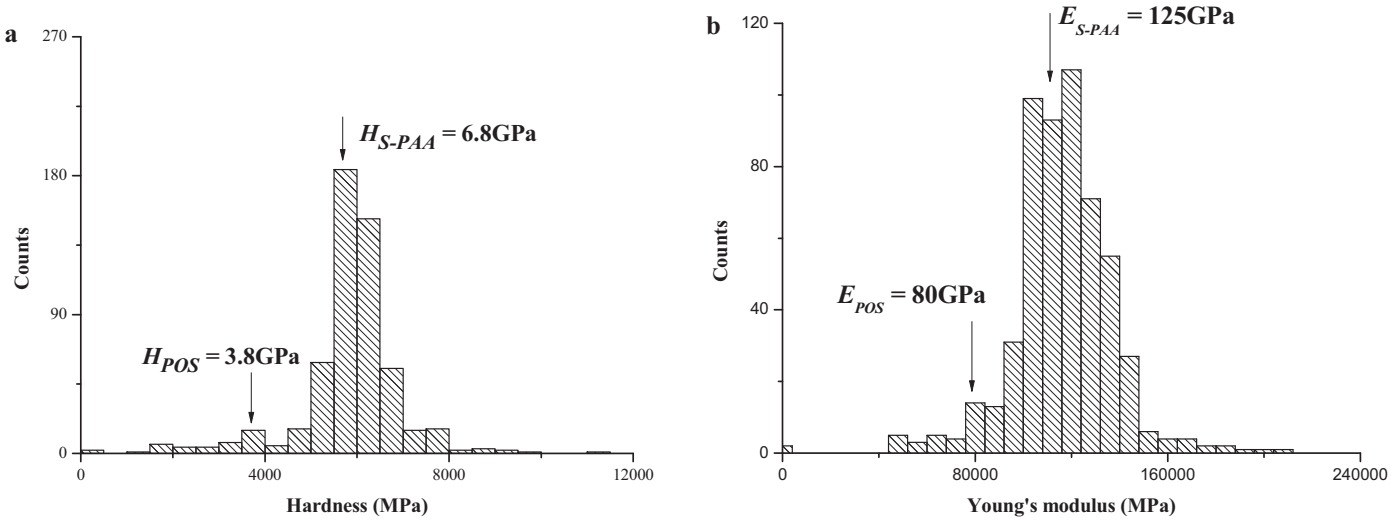

Fig. 8. Histogram representation of the different experimental values using a constant bin size of 500 MPa: (a) hardness and (b) Young's modulus.

(the equations and the tip employed), the presence of indentation size effect [30–32] due to the strain gradient plasticity activated near the imprint and to small differences among the different porous anodic films. The S-PAA hardness is also over three times lower than that observed in dense α-alumina, reasonably if we take into account the porosity of the films. On the other hand, mechanical data of POS cannot be compared with bibliographic results, as this is the first time that the mechanical properties of these structures generated under burning conditions are studied.

4. Conclusions

Novel results on the utilization of nanoindentation to investigate the nanomechanical properties of heterogeneous materials were presented. In particular, hardness and Young's modulus of POS and S-PAA formed during aluminium anodizing in sulphuric acid under burning conditions were measured and associated with the composition and structure of these oxide structures. We demonstrated that the nanoindentation technique is useful to extract the mechanical behaviour of small volumes of heterogeneous materials, where the hardness and Young's modulus are unknown. In this way, a statistical method was used to clarify and isolate the mechanical properties of each phase, without visualizing the residual imprints using optical methods. In order to obtain quantitative information of these parameters the CDF method was applied to analyze the experimental values.

The results indicated that the hardness and Young's modulus of POS are factors of about 1.6–1.8 times lower than those of S-PAA, indicating that POS have lower mechanical properties associated with their different chemical composition and structure. The results would also indicate that porous anodic alumina that surrounds the POS (POS/S-PAA$_{interface}$) presents a degradation of their mechanical properties, probably due to mechanical stresses arising from the expansionary forces originated by the rapid oxide growth of POS in relation with S-PAA.

Acknowledgement

This paper was supported by contract MAT-2006-12913 from the Spanish MCINN and the European Regional Development Fund.

References

[1] A.W. Brace, 75 years of sulphuric acid anodizing, Transactions of the Institution of Metal Finishing 80 (2002) 177–182.
[2] P.G. Sheasby, R. Pinner, 6th ed., The Surface Treatment and Finishing of Aluminum and its Alloys, vol. 1, Finishing Publications Ltd./ASM International, UK, 2001.
[3] B.A. Scott, Decorative and protective finishes produced on aluminium by hard anodizing, Transactions of the Institution of Metal Finishing 43 (1965) 1–8.
[4] I. De Graeve, H. Terryn, G.E. Thompson, Influence of local heat development on film thickness for anodizing aluminum in sulfuric acid, Journal of the Electrochemical Society 150 (2003) B158–B165.
[5] S. Ono, M. Saito, H. Asoh, Self-ordering of anodic porous alumina induced by local current concentration: burning, Electrochemical and Solid-State Letters 7 (2004) B21–B24.
[6] S. Ono, M. Saito, M. Ishiguro, H. Asoh, Controlling factor of self-ordering of anodic porous alumina, Journal of the Electrochemical Society 151 (2004) B473–B478.
[7] T. Aerts, I. De Graeve, H. Terryn, Study of initiation and development of local burning phenomena during anodizing of aluminium under controlled convection, Electrochimica Acta 54 (2008) 270–279.
[8] T. Aerts, I. De Graeve, G. Nelissen, J. Deconinck, S. Kubacki, E. Dick, H. Terryn, Experimental study and modelling of anodizing of aluminium in a wall-jet electrode set-up in laminar and turbulent regime, Corrosion Science 51 (2009) 1482–1489.
[9] T. Aerts, I. De Graeve, H. Terryn, Control of the electrode temperature for electrochemical studies: a new approach illustrated on porous anodizing of aluminium, Electrochemistry Communications 11 (2009) 2292–2295.
[10] T. Aerts, J.B. Jorcin, I. De Graeve, H. Terryn, Comparison between the influence of applied electrode and electrolyte temperatures on porous anodizing of aluminium, Electrochimica Acta 55 (2010) 3957–3965.
[11] T. Aerts, I. De Graeve, H. Terryn, Anodizing of aluminium under applied electrode temperature: process evaluation and elimination of burning at high current densities, Surface and Coatings Technology 204 (2010) 2754–2760.
[12] B. Gastón-García, E. García-Lecina, J.A. Díez, M. Belenguer, C. Müller, Local burning phenomena in sulfuric acid anodizing: analysis of porous

anodic alumina layers on AA1050, Electrochemical and Solid-State Letters 13 (2010) C33–C35.
[13] W.C. Oliver, G.M. Pharr, An improve technique for determining hardness and elastic modulus using load and displacement sensing indentation technique, Journal of Materials Research 7 (1992) 1564–1583.
[14] A.C. Fischer-Cripps, Nanoindentation, Springer-Verlag, New York, NY, 2002.
[15] J.J. Kim, Y. Choi, S. Suresh, A.S. Argon, Nanocrystallization during nanoindentation of a bulk amorphous metal alloy at room temperature, Science 295 (2002) 654–657.
[16] G. Constantinides, F.-J. Ulm, K. Van Vliet, On the use of nanoindentation for cementitious materials, Materials and Structures 36 (2003) 191–196.
[17] N.X. Randall, M. Vandamme, F.-J. Ulm, Nanoindentation analysis as a two-dimensional tool for mapping mechanical properties of complex surfaces, Journal of Materials Research 24 (2009) 679–690.
[18] G. Constantinides, F.-J. Ulm, The nanogranular nature of C–S–H, Journal of the Mechanics and Physics of Solids 55 (2006) 64–90.
[19] G. Constantinides, K.S. Ravi Chandran, F.-J. Ulm, K.J. Van Vliet, Grid indentation analysis of composite microstructure and mechanics: principles and validation, Materials Science and Engineering A 430 (2006) 189–202.
[20] V. Canseco, J.J. Roa, E. Rayón, A.I. Fernández, E. Palomo, Mechanical characterization at nanometric scale for heterogeneous graphite–salt phase change materials with a statistical approach, Ceramics International (2011), doi:10.1016/j.ceramint.2011.07.021.
[21] E. Rayón, V. Bonache, M.D. Salvador, J.J. Roa, E. Sánchez, Hardness and Young's modulus distribution in atmospheric plasma sprayed WC-Co coatings using nanoindentation, Surface and Coatings Technology 205 (2011) 4192–4197.
[22] J.M. Montero-Moreno, M. Sarret, C. Müller, Influence of the aluminum surface on the final results of a two-step anodizing, Surface and Coatings Technology 201 (2007) 6352–6357.
[23] I. Horcas, R. Fernández, J.M. Gómez-Rodríguez, J. Colchero, J. Gómez-Herrero, A.M. Baro, WSxM: a software for scanning probe microscopy and a tool for nanotechnology, Review of Scientific Instruments 78 (2007), 013705/1–013705/8.
[24] J.J. Roa, X.G. Capdevila, M. Martínez, F. Espiell, M. Segarra, Determination of hardness, Young's modulus of YBCO samples textured by the Bridgman technique, Nanotechnology 18 (2007), 385701/1–385701/6.
[25] W.C. Oliver, G.M. Pharr, Measurement of hardness and elastic modulus by instrumented indentation: advances in understanding and refinements to methodology, Journal of Materials Research 19 (2004) 3–20.
[26] J.J. Roa, E. Jiménez-Piqué, T. Puig, X. Obradors, M. Segarra, Nanoindentation of multilayered epitaxial $YBa_2Cu_3O_{7-\delta}$ thin films and coated conductors, Thin Solid Films 519 (2011) 2470–2476.
[27] F.J. Ulm, M. Vandamme, C. Bobko, J. Alberto Ortega, K. Tai, C. Ortiz, Statistical indentation techniques for hydrated nanocomposites: concrete, bone and shale, Journal of the American Ceramic Society 90 (2007) 2677–2692.
[28] Z. Xia, L. Riester, B.W. Sheldon, W.A. Curtin, J. Liang, A. Yin, J.M. Xu, Mechanical properties of highly ordered nanoporous anodic alumina membranes, Reviews on Advanced Materials Science 6 (2004) 131–139.
[29] G. Alcalá, P. Skeldon, G.E. Thompson, A.B. Mann, H. Habazaki, K. Shimizu, Mechanical properties of amorphous anodic alumina and tantala films using nanoindentation, Nanotechnology 13 (2002) 451–455.
[30] W.D. Nix, H. Gao, Indentation size effects in crystalline materials: a law for strain gradient plasticity, Journal of the Mechanics and Physics of Solids 46 (1998) 411–425.
[31] J.G. Swadener, E.P. George, G.M. Pharr, The correlation of the indentation size effect measured with indenters of various shapes, Journal of the Mechanics and Physics of Solids 50 (2002) 681–694.
[32] J.J. Roa, A. Magrasó, M. Morales, P. Núñez, M. Segarra, Determination of hardness, Young's modulus and fracture toughness of lanthanum tungstates as novel proton conductors, Ceramics International 37 (2011) 1593–1599.